Implementation and Evaluation of Patient-Specific Three-Dimensional Internal Dosimetry

Katherine S. Kolbert, George Sgouros, Andrew M. Scott, James E. Bronstein, Rachel A. Malane, Jiaju Zhang, Hovanes Kalaigian, Stephen McNamara, Lawrence Schwartz and Steven M. Larson

Department of Medical Physics and Department of Radiology, Nuclear Medicine Service, Memorial Sloan-Kettering Cancer Center, New York, New York; Ludwig Institute/Austin Hospital, Australia; University of Pennsylvania, Pennsylvania; and Frank J. Scallon Medical Science Foundation Fellow, Princeton University, New Jersey

Current methods for calculating the absorbed dose in a target region from a source region rely on a standard "reference man" geometry and assume an uniform distribution of radiolabel. While this approach is acceptable at the low levels of radioisotope administered for most diagnostic purposes, the generality of the calculations is not adequate for doses at the higher levels required for therapy and is not easily extendible to tumor dosimetry. **Methods:** We have developed an integrated system which utilizes patient anatomy and radionuclide distribution in the calculation of absorbed dose rate or total dose to any user-defined target region. Images of radionuclide distribution (PET/SPECT) are registered to anatomic images (CT/MRI) and then entered into a three-dimensional internal dosimetry software system (3D-ID) where regions of interest are defined. Dose calculations are performed by the mathematical convolution between a user-specified, dose-point kernel with the activity in the source volume over the target volume. The resulting dose rate distribution may be scaled by cumulated activity to yield absorbed dose. In addition to calculating the mean dose, dose-volume histograms may be generated which plot absorbed dose with respect to percent of volume. The method was evaluated using selected standard man phantom organs. **Results:** Dose estimates for two patient studies are included to illustrate differences between patient-specific and MIRD-based calculations. The package provides an alternative approach to image display and three-dimensional internal dose calculations. **Conclusion:** The dose-volume histogram representation of absorbed dose to a target volume provides valuable information in assessing tumor control probability and normal tissue toxicity.

Key Words: three-dimensional dosimetry; radionuclide therapy; dose-volume histograms

J Nucl Med 1997; 38:301–308

The conventional and established methodology for calculating the mean absorbed dose from a source organ to a target organ utilizes the MIRD S-factor formalism, which requires that individual source organs be homogeneous, of uniform density and unbounded (*1–3*). In addition, the organ geometry used for the source and target organs relies on reference or standard geometries in which the various human organs have been determined to be of specific sizes. The mean absorbed dose in a target organ is then calculated using these idealized organs by summing the contribution from each source organ multiplied by the source cumulated activity. The cumulated activity is typically obtained by integrating kinetic data acquired from the collection of serial blood and total-body imaging.

The deposition of energy in a source region is affected by the distribution of source activity and by the size, shape and geometric relationship of the source and target organs. The use of standard man and the assumption of uniformity has generally not been considered a problem in the diagnostic use of internal emitters because of the low activity being used. At the higher level of activity that is required for therapeutic use, more accurate dose calculations may be required. In addition, since the location, size and shape of tumor tissue is not known in advance, it is not possible to assemble tables of S-factors for tumors. A variety of approaches have been developed to address these needs (*4,5*).

Depending on the radionuclide, size, shape and location of a tumor, and the activity in adjacent organs, the absorbed dose to a tumor may be obtained by considering only electron self-dose. This estimate may be improved upon if the tumor may be assumed to be a sphere or ellipsoid. In such cases additional terms representing self-dose photon contributions may be included using absorbed fractions listed in MIRD Pamphlet No. 5 (*2*). This approach has been implemented in the MIRDOSE3 program (*6*). These techniques do not provide estimates to normal tissue dose from activity in the tumor and do not include the contribution to tumor dose from activity in adjacent normal tissues. A more detailed calculation of tumor and adjacent tissue dose may be obtained using MABDOSE, a software package in which the user is allowed to introduce tumors of regular geometries within the standard geometry (*7*). The modified geometry is then used in a Monte Carlo calculation which provides tumor-associated S-factors.

Other approaches, which provide more detailed and patient-specific absorbed dose estimates, generally require a three-dimensional representation of patient anatomy as well as the radioactivity distribution within individual organs or regions of a specific patient. The radioactivity distribution has been obtained from SPECT, PET and biopsy samples (*8,9*). Anatomical information, which is used to define tumor and normal organ size and position has been obtained from CT or MR imaging. Patient-specific methods may be categorized as point-kernel (*8,10–12*) or Monte Carlo-based (*13,14*). A distance-histogram technique has also been described (*15*). In almost all cases, these methods have been implemented for phantom studies or for a select number of patients.

In order to perform patient specific dosimetry, it is necessary to have: the appropriate patient image files available for display, a method for analysis and region of interest (ROI) definitions, a method for dosimetric calculation and the ability to analyze the results of the dose calculation. Images may come from a variety of sources in a variety of formats. The logistics of obtaining them is complicated by the lack of inter- and intra-image modality standards. While the elements of image registration, display, ROI definition and dose calculation exist separately to some extent, these steps have not been incorpo-

Received Feb. 7, 1996; revision accepted May 29, 1996.

For correspondence contact: Katherine S. Kolbert, MS, Nuclear Medicine Service, 1275 York Ave., New York, NY 10021.

For reprints contact: George Sgouros, PhD, Dept. of Medical Physics, 1275 York Ave., New York, NY 10021.

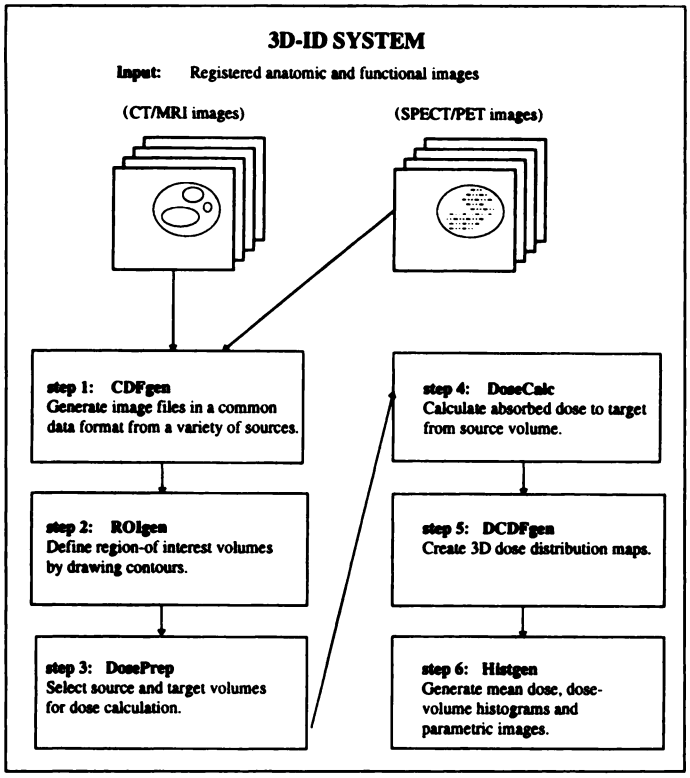

FIGURE 1. The 3D-ID system flowchart shows the input of registered functional and anatomic images. Each subsequent box describes a separate software module sharing the same interactive interface except for the dose calculation step which is carried out in batch mode.

rated into a comprehensive system. The current work is intended to address this need.

MATERIALS AND METHODS

General

The methodology expands upon the concept of using CT/MRI and SPECT/PET images for dose calculation and dose-volume histograms for dose representation described by Sgouros et al. and Kolbert et al. (*8,10,16,17*). The system, which is modular, extensible and uses a common interface, consists of six separate software programs (Fig. 1). The first three steps collect and prepare regions for the fourth step, the dose calculation. The final two steps allow for an analysis of the dose distribution and the mean absorbed dose by depicting the spatial dose distribution as a series of images and generating dose-volume histograms. With the exception of the dose calculation module (coded in C), 3D-ID is written in Interactive Data Language (IDL), (Research Systems Inc., Boulder, CO). 3D-ID is platform-independent and can be run on any system that has an IDL license; it has run on SUN SPARCstations, DEC VAXstations, DEC AXP Alpha workstations and personal computers.

Image Acquisition, Registration and Format

Images can be obtained either directly by digital means or by digitizing film. The nontrivial issues of image acquisition and registration have been kept separate from the software system in order to keep the focus of this work on the logistics of image handling, ROI definition and dose calculation.

The first software module, Common Data Format generator (CDFgen) in the 3D-ID system converts input two-dimensional images into a three-dimensional common data format. Since patient images come from a variety of sources in a variety of vendor formats with and without header data, we created our own header to describe the patient, study and image characteristics (Table 1). The header elements represent a minimal set to reconstruct the

TABLE 1
3D-ID Image Header Data

Patient	Study	Image
Name	Modality (CT, MRI, PET, SPECT)	x, y, z spacing (regular or irregular)*
Identification	Isotope (multiple isotopes are acceptable)	x, y, z step size (voxel dimension)
	Body part imaged	x, y, z units
	Agent used for imaging	
	Diagnosis	

*Irregular z spacing currently not supported by 3D-ID.

image. The header, along with the three dimensional image data are stored as network Common Data Format (netCDF) files (*18*). NetCDF was chosen primarily because image and header data can be handled in a network and platform transparent manner.

Using an interface that repeats common menu elements throughout the other interactive modules of 3D-ID, CDFgen allows the user to select the format of the images from a list of implemented formats. Currently, CDFgen can read two-dimensional image slices that were created on either UNIX or VMS operating systems as well as three-dimensional images that are already in netCDF with the elements defined in Table 1. A series of pop-up lists are provided for the users to select the appropriate agent, diagnosis, body part and isotope associated with the study (Fig. 2).

It is necessary to provide the slice spacing and pixel x and y dimensions to CDFgen so that accurate calculations based on the image elements can be made. When images are digitized from film, the size of an individual pixel will depend on the settings used during digitization. An interactive submodule of CDFgen recalibrates the image pixel dimension by calculating the distance between evenly spaced points selected by the user. The size scale on the film is typically used for this purpose.

ROIs: Definition and Selection

Once images are entered into the 3D-ID system, the ROIs that will be used in the dose calculation are defined using the ROI generator (ROIgen) module. In ROIgen, the three-dimensional image sets are arranged in two lines corresponding to an anatomical modality (CT/MRI) and to a radionuclide modality (SPECT/PET) (Fig. 3). By displaying images separately rather than in fused or overlaid display mode, all available data from both modalities is preserved. Other features of the program include independent control of each modality's color scale, the ability to view the images in a cine mode, zoom capabilities and the assessment of volume and total counts of a three-dimensional ROI.

Contour drawing is performed in a side-by-side, dual modality display of individual image slices. As a result, information from both imaging modalities can be utilized while drawing contours. Before drawing, the cursor appears over both images so that the user can easily identify corresponding points within the two images. In addition, the coordinates and value of any point in either image may be displayed. In Figure 3, for instance, the tumor is visible in both modalities, although it is more clearly seen in the SPECT image. It would not be possible, however, to draw the liver from the SPECT image alone. Contours may be drawn using either image and it is possible to switch back and forth between images during drawing

After the volumes have been defined, they may be identified as source or target for a particular dose calculation using Dose Preparation (DosePrep). If multiple processors or multiple workstations are available, the dose calculation can be divided into a

FIGURE 2. The set of 25 two-dimensional SPECT registered and resliced images from the HuM195 patient study (Patient 1) as displayed in CDFgen. The pop-up dialog shows part of the list of diagnoses. Image display has been selected at 1/2 the original image size.

number of individual parallel batch jobs; the user may select the operating system for the dose calculation (currently UNIX or VMS) and the resulting batch file will be appropriately defined.

It is also necessary to indicate the radionuclide used for the dose calculation. If more than one radionuclide was used for imaging and/or therapy, then dose calculations for multiple isotopes can be specified.

DosePrep uses the contours drawn in ROIgen to create a patient-specific source and target volume, which excludes all activity outside the defined source or target region for the purposes of the dose calculation.

Dose Calculation

The dose calculation (DoseCalc) program utilizes user-specified dose point kernels which are convolved with the activity or cumulated activity in the source volume to generate dose rate or dose values for each voxel in the target volume. The point kernel for a radionuclide is essentially a table of absorbed dose versus

FIGURE 3. ROIgen multi-image display shows patient study with contours defined for outer (magenta; drawn by adjusting the contrast level of the images), liver (light blue), tumor 1 (green) and tumor 2 (yellow). Independent color temperature controls appear below the two rows of images.

distance from a point source in a specific medium. The point kernels currently being used by 3D-ID have been generated by Monte Carlo simulation of photon spectrum transport through water (*19*). Since each radionuclide spectrum was simulated in the generation of these kernels, interpolation between photon energies was not necessary. For details regarding the point-kernels see reference *19*. The electron dose is deposited within the activity containing voxel for most human dosimetry calculations. If the electron range is significant relative to patient organ dimensions, an electron point-kernel may be added to the early portion of the photon point-kernel to account for the spatial distribution of the electron dose deposition (*20–22*).

The convolution has been implemented by iterating over the entire source and target volume. For every none-zero source voxel value, the distance to every target voxel is calculated and looked up in the point-kernel table. The resulting value is multiplied by the activity in the source voxel. If the distance value is not found in the table, a linear interpolation is carried out. The resulting value is added to an array of dose values within the target region. When the point in the source coincides with the target point, the total energy associated with electron emissions is deposited in that voxel if the electron contribution is not included in the point-kernel.

The resulting arrays of dose numbers are essentially images of dose distribution and can be viewed as "maps" of the spatially varying dose in a target volume from a particular source volume or volumes. The modular characteristic of 3D-ID provides the flexibility to replace the current dose calculation technique with other techniques that may be either point-kernel or Monte Carlo based. A fast Fourrier approach to the convolution has not been implemented in the point-kernel technique that is currently used to allow for future implementation of density corrections using an effective path length scheme as described previously (*10*).

The amount of computer time necessary for a particular dose calculation depends upon a number of factors, including the number of source and target pixels, "granularity" of the point kernel (i.e., how many interpolations are performed), and speed of the computer on which it is run. Assuming that m is the number of source pixels and n is the number of target pixels, the average running time for the point-kernel distance lookup (which is carried out using a binary search technique) is of the order of $\log(n)$ and the average running time of the entire dose calculation is of the order of $mn\log(n)$.

Once the calculation has been performed, the next step is performed by dose CDF file generator (DCDFgen) which creates a three-dimensional absorbed dose dataset for further display and analysis of the dose data.

Dose Summary and Analysis

The final step in the 3D-ID process is histogram and summary generator (HistGen) which calculates the mean absorbed dose to a target per unit cumulated activity from a source (or sources). It also generates dose-volume histograms of source to target regions in order to summarize the dose information in a clinically interpretable manner. Additionally, it presents all image data in a summary display of anatomic, functional and dose distribution images.

If absorbed dose instead of dose-rate is desired and time-sequential SPECT or PET studies are unavailable, the absorbed dose in each target voxel may be scaled by a total source organ cumulated activity that is typically obtained from planar imaging kinetics. In this way, the spatial distribution of activity is assumed to be preserved throughout the study period. This is a first-order approximation which may be improved upon if additional (three-dimensional) pharmacokinetic data are obtained. Cumulated activity estimation is external to the system as this will depend upon the details of patient imaging and pharmacokinetic data acquisition.

The mean dose over a target volume is determined by taking the mean of all values in the dose array. Dose-volume histograms are also generated from the dose array. The information may be plotted as either an integral or differential plot. In the former, the percent of volume receiving less than or equal to a particular dose value is plotted as a function of the dose value. In the latter, the percent of volume receiving a particular absorbed dose range is plotted compared with the dose range.

Evaluation of Method

In order to evaluate the accuracy of 3D-ID dose calculations, images of selected organs were generated using the equations describing the mathematical phantoms for standard human geometries described in MIRD Pamphlet No. 5, Revised and in the Cristy-Eckerman phantom series (*2,23*). Phantoms for the spine, liver, pancreas and spleen were created with pixel size of 0.14×0.14 cm^2, slice spacing of 0.5 cm by assigning a uniform activity to each pixel that satisfied the mathematical phantom. Agreement between 3D-ID generated volumes and MIRD Reference Man organs (*2*) ranged between 1.9% and 4.8%.

The phantom images were read into the 3D-ID system as described above by CDFgen. Since the images generated were binary images, ROIs were determined in ROIgen using a simple, edge-following routine (*24*)

In DosePrep, all combinations of pancreas, spleen and liver were selected as source and target ROIs to calculate self-dose and cross-organ dose (Fig. 4). In particular, the pancreas to spleen cross-organ dose calculation was chosen because of the lack of intervening bone. This allowed for evaluating 3D-ID without considering the attenuating effect of different tissue densities. Dose estimates were performed for ^{131}I using a previously published point-kernel (*19*). The DoseCalc program was run on three types of Alpha DEC workstations: DEC server 2100 (190 MHz), DEC 3000-*M*400 (130 MHz) and DEC 3000-*M*600 (175 MHz). The choice of which workstation to use was based upon availability.

Using the Histgen program, the mean dose and dose-volume histograms for the phantom organs were generated. By assigning a value of 1 as cumulated activity to a source, the mean dose reported by Histgen is equivalent to a source-target S-factor.

Clinical Implementation

To illustrate the use of the software system, 3D-ID dosimetry was performed on two patients from two separate protocols. The first patient, with leukemia, was injected with trace-labeled monoclonal antibody ^{131}I HuM195. For details regarding the antibodies and patient studies see reference *25*. One to two days before antibody administration, CT images of the patient were obtained over the abdomen; SPECT images were obtained 2 days after antibody administration. The CT study was performed on a General Electric Advance scanner (Milwaukee, MN). SPECT was performed on a dual-headed Adac Pegasys scanner (Milpitas, CA). The CT and SPECT images were transferred digitally into a DEC Vaxstation 4000 (Maynard, MA). The SPECT images were exported (using ADAC supplied routines) into Interfile format and then translated into individual 2D $256 \times 256 \times 256 \times$ 16-bit slices using in-house developed software routines. They were then registered to the CT images using image registration software developed by Pelizzari and Chen (*26*).

3D-ID was then used to estimate the self-absorbed dose to the liver and the spleen in the following manner. After the images were acquired and registered, they were placed into the 3D-ID system by using CDFgen to read them from the Vaxstation, convert them into the common format, and enter study descriptive information. Using the ROIgen program, contours were drawn in order to define the liver and spleen. The 3D CT, SPECT and ROI datasets were read into DosePrep. The liver and then the spleen were selected as both

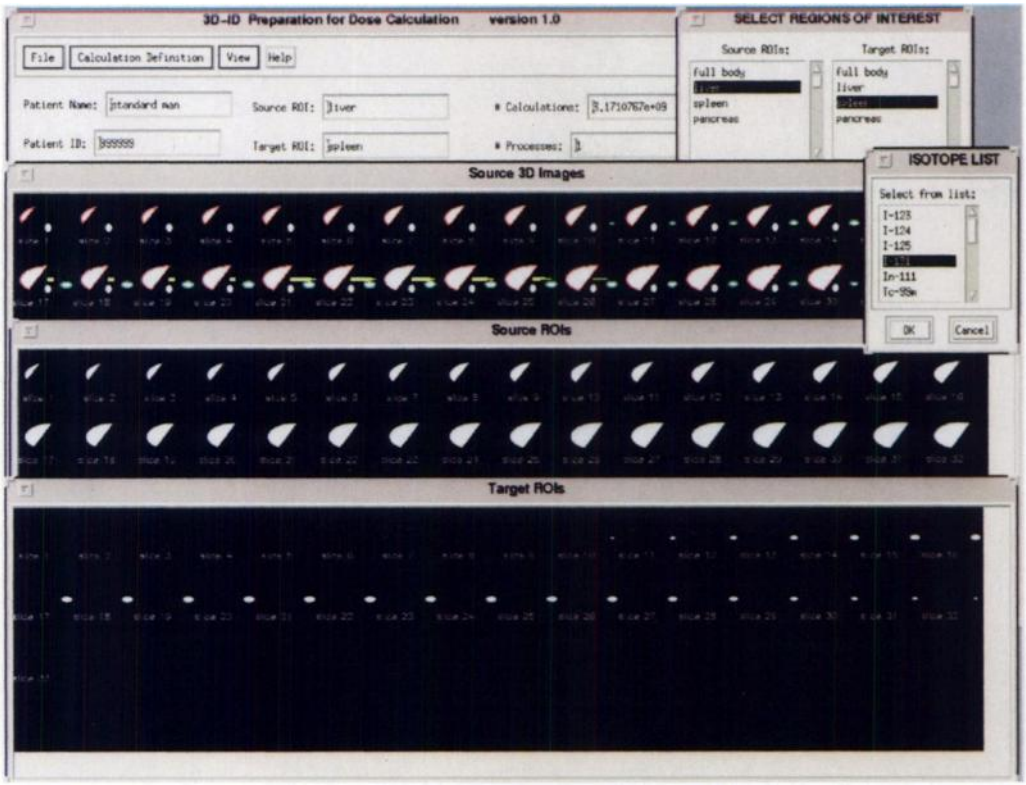

FIGURE 4. Using DosePrep, a liver-to-spleen dose calculation for the phantom study using ^{131}I has been selected. The program visually confirms the choice of source and target by displaying the selected regions.

source and target regions. The liver and spleen calculations were divided into five and four sets of VMS processes, respectively. Batch process jobs and image sets were transferred to the appropriate workstations and the calculations carried out using DoseCalc. The resulting dose distribution maps were recombined using DCDFgen and read into HistGen. The voxel values for each source region in the SPECT study were converted to cumulated activity using planar imaging kinetics obtained during the patient study. Briefly, kinetics for each organ were obtained by drawing contours on a series of planar images. The net counts in each contour were corrected for attenuation and scatter as described previously (*25,27*). The resulting time-activity curves for each source organ were fit to a decreasing exponential function and integrated analytically to yield cumulated activity for each source organ. The cumulated activity values were then entered into Histgen. Histograms representing the spatially varying dose distribution as well as the mean dose to each organ were generated. After obtaining the local mean dose values for liver and spleen, the contribution from the remainder of the body was added using MIRD S-factor values as described in reference *3*.

The second patient, with metastatic colorectal carcinoma, was injected with ^{131}I labeled CC49 antibody. For details concerning this study and the antibody see reference *28*. CT images were obtained by digitizing film using an image capture board installed on a PC. SPECT and planar images were obtained as in the above study. After image registration (*29*), the CT and resliced SPECT images were entered into the 3D-ID system using CDFgen. In this case, the voxel size of the CT images had been lost in digitization, so it was necessary to use the recalibration module of CDFgen accessed by pressing the "calculate" button (Fig. 2). Using the cursor to indicate equally spaced points on the embedded scale on the CT, a pixel size of 0.18 cm was assigned in both x and y directions. The 1-cm slice spacing of the registered image sets was also assigned.

Contours were drawn and ROIs were defined for the liver and two lesions within the liver (Fig. 3). As described above, CT, SPECT and region-of interest datasets were read into DosePrep. In this case, it was desirable to obtain not only liver and tumor self-dose, but also the dose to the liver from the two tumors and the tumor dose from activity in the liver. By sequentially indicating each of the three regions as source and then as target, a series of processes were created simply by highlighting the appropriate name in the source and target list. Tumor-associated activity was subtracted from the liver using an image subtraction program in which the tumor ROIs were used to remove the voxels representing tumor activity, thereby leaving only normal liver tissue for dose calculations. The resulting processes and the appropriate datasets were transferred to a series of DEC Alpha workstations and the dose calculations carried out by submitting the calculation as nine batch jobs. As above, the resulting dose distribution maps were recombined using DCDFgen and read into HistGen. As in the previous patient study, histograms representing the spatially varying dose distribution as well as the mean dose to each organ were obtained. The contribution from the rest of the body was added as before.

RESULTS/DISCUSSION

Comparison with MIRD S-Factors

Results of the phantom study for liver, pancreas and spleen are summarized in Table 2. Agreement between MIRD and 3D-ID values for organ self-dose ranged between 0.8% and 5%; these errors are typically within the s.d. associated with the S-factor values reported in MIRD Pamphlet No. 11. These differences may also be due to the differences in volume obtained when the standard phantom organs are represented by a discrete matrix.

The pancreas self-dose S-factor was a significant exception to this. As shown in Table 2, the 3D-ID result differed from the MIRD value by 46%. This is very likely due to an inconsistency in the MIRD data. The electron dose to the pancreas, without including photon contributions, yields an ^{131}I self-dose S-factor that is approximately 6.72×10^{-3} rad/μCi-hr which is already greater than the listed MIRD S-factor. The equations used to

TABLE 2
Comparison of S-Factor Values Arrived at Using MIRD Method and 3D-1D Method for Iodine-131

Tissue ROIs		S-factors*			MIRD:3D-ID S-factor comparison % diff
Source	Target	MIRD (rad/μCi hr)	3D-ID (rad/μCi hr)	MIRDOSE3 (rad/μCi hr)	
Liver	Liver	3.00E-04	2.85E-04	2.82E-04	5.0
	Pancreas	1.20E-05	1.19E-05	1.36E-05	0.8
	Spleen	3.00E-06	3.54E-06	2.86E-06	18.0
Pancreas	Liver	1.20E-05	1.19E-05	1.36E-05	0.8
	Pancreas	4.70E-03	6.87E-03	4.74E-03	46.2
	Spleen	5.40E-05	5.66E-05	4.77E-05	4.8
Spleen	Liver	2.70E-06	3.54E-06	2.86E-06	31.1
	Pancreas	5.40E-05	5.66E-05	4.77E-05	4.8
	Spleen	2.60E-03	2.66E-03	2.57E-03	2.3

*Traditional units used for comparison.

describe the MIRD pancreas yield a mass that is approximately consistent with the mass listed in MIRD Pamphlet No. 11. The electron dose results suggest, however, that a different mass was used in obtaining the S-factor listed in MIRD Pamphlet No. 11. We repeated the 3D-ID calculation using the Cristy-Eckerman phantom equations and came within 5% of the listed S-factor.

The difference between 3D-ID and MIRD cross-organ S-factor values ranged from 0.8% to 31%. The greatest difference was observed between liver and spleen values. It is of interest that the MIRD liver to spleen S-factor is different from the spleen to liver S-factor. In both the 3D-ID and the Cristy-Eckerman calculations, reciprocity holds for these two organs. The error associated with liver-spleen S-factor calculations may reflect a fundamental limitation in the point-kernel approach. Both of these organs are near the periphery of the abdomen and are therefore subject to a diminished backscatter exposure since photon emissions that reach outside of the body will not be backscattered. Since the point-kernel is obtained assuming an infinite medium, the dose at each point is obtained assuming complete backscatter of all emissions. It follows that a point-kernel calculation would overestimate the absorbed dose to an organ adjacent to the body surface. This is consistent with the liver-spleen results and with the S-factors obtained for the pancreas. The error associated with the pancreas to liver S-factor is less than that associated with the pancreas to spleen S-factor. Since the pancreas (the source organ) is centrally located, the absorbed dose to liver is less likely to be underestimated due to backscatter loss because, although still at the periphery of the body, it is larger than the spleen.

Clinical Results

The image tableau generated by Histgen (Fig. 5) provides a visual summary consisting of both modalities imaged for Patient 1, the ROIs on the individual transverse slices and the dose distribution maps obtained from the dose calculation.

Dose estimates obtained for the two patient studies are listed in Table 3 In the dose calculation for liver and spleen, the dose contributions from other organs and from the remainder of the body, as obtained using the S-factor methodology, were added

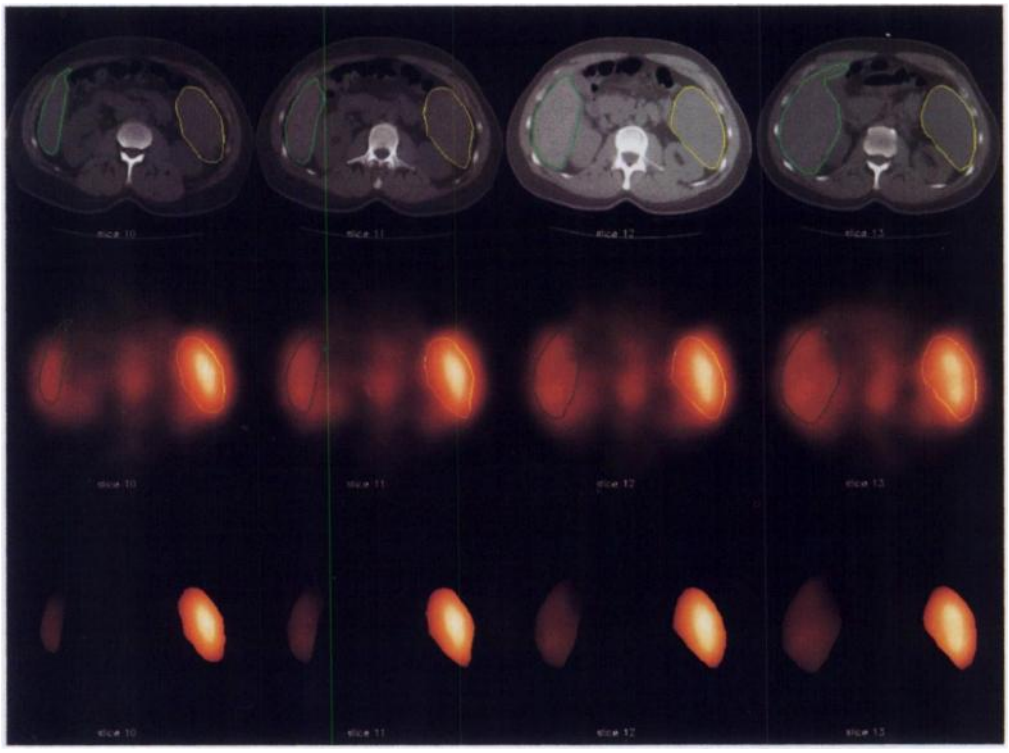

FIGURE 5. The multimodality image display in HistGen showing slices 10–13 for Patient 1. CT images show contours for the liver (green) and spleen (yellow) (top row). The corresponding resliced SPECT images (middle row). Dose distribution maps for liver self-dose and spleen self-dose (bottom row).

TABLE 3
Comparison of MIRD and 3D-ID Dose in Patient Studies

Patient no.	Tissue	% Difference in volume reference man: patient specific	Dose* MIRD (cGy/mCi)	Dose* 3D-1D (cGy/mCi)
1	Liver	24.43	0.77	1.02
	Spleen	252.98	4.9	1.74
2	Liver	10.16	0.45	0.59
	Tumor 1	na	7.13†	7.39
	Tumor 2	na	4.91†	5.20

*Liver and spleen doses include a remainder of body term.
†Obtained assuming local deposition of electrons.
na = not applicable.

to the self-dose estimate. In Patient 1, injected with ^{131}I-HuM195, the 3D-ID liver dose is 24.5% greater than the MIRD-derived estimate and the spleen value is 3.9-fold less. The large spleen discrepancy may be explained by the large difference in the volume of the spleen (Table 3). Due to their leukemia, almost all the patients in the protocol from which this patient was selected exhibited splenomegaly. If the MIRD estimates of the absorbed dose for both liver and spleen are scaled according to mass, the difference in liver absorbed dose is within 1% but the spleen absorbed dose differs by 20%.

For Patient 2, injected with ^{131}I-CC49, the liver absorbed dose between the two methods differs by 31.8% without mass adjustment; if the MIRD value is adjusted for actual liver mass, the values differ by 12%. 3D-ID estimates of tumor dose are compared with estimates obtained by considering electron dose deposition only, and assuming all electron energy is locally deposited; the values differ by 3.5% and 5.6%, for the 71.2 and 160.3 g tumors, respectively.

Integral dose-volume histograms for Patient 1 and Patient 2 is shown in Figure 6. It may be seen in the histograms for Patient 1 (Fig. 6A) that liver self-dose ranges from 0.2 cGy/mCi to 1.0 cGy/mCi and spleen dose ranges from 0.4 cGy/mCi to 2.1 cGy/mCi. This range of dose values is not revealed by the mean self-dose of 0.77 cGy/mCi for liver and 1.5 cGy/mCi for spleen. Depending upon each organ's prior exposure to radioactive or chemotherapeutic agents the dose distribution may have an impact on organ toxicity. Dose volume histograms of tumors are particularly important since treatment failure is most likely caused by underdosing a portion of the tumor volume. A first-order assessment of potential treatment efficacy may be obtained by simply examining the minimum tumor dose shown on the histogram. If this value is below that required for tumor control, it is unlikely that treatment will be successful even if the mean dose is greater than that required for tumor control.

Calculation Time

The time required to draw the contours is dependent on the skill and experience of the person drawing the contours—a person familiar with 3D-ID and anatomic/functional details of the image can draw several contours per minute. The total time required to define a ROI is therefore a function of the skill level of the person doing the drawing, the number of ROIs per image set and the number of slices over which the region is being defined.

A total of 13 hr were required for the dose calculations associated with Patient 1 (voxel size $0.1285 \times 0.098 \times 1$ cm^3). The calculation was divided into nine processes, so that no individual process took more than 3 hr. Individual dose calculations for Patient 2 (voxel size $0.176 \times 0.176 \times 1$ cm^3) ranged from 20 sec for tumor 1 self-dose to 1 hr 51 min for liver self-dose. The total time taken for the entire dose calculation for Patient 2 was 2 hr and 35 min. If multiple workstations are not available and the calculations cannot be run concurrently, the calculation time is not prohibitive since the calculations may be run in the background or overnight.

Since the dose calculation technique may be changed due to the modular design of 3D-ID, no further effort has been made to increase the efficiency of these calculations.

CONCLUSION

We have developed a series of software modules that address the logistical issues associated with patient-specific three-dimensional dosimetry. Software tools have been developed which combine images from different modalities, define ROIs using available multimodality data and identify source and target volumes for dosimetry. We have implemented a point-kernel based dosimetry calculation and several different approaches for displaying the spatial distribution of absorbed dose in a biologically pertinent manner. The dose calculation is carried out in a separate module so that different calculation schemes, including Monte Carlo, may be used with 3D-ID. The point kernel based comparisons with MIRD S-factors have revealed certain internal inconsistencies in the MIRD S-factors and may have also pointed out a basic weakness in the point-kernel based approach. The methodology has been applied to patient studies and in the two illustrative cases included in this work, we have shown how the spatial distribution of absorbed dose as represented by dose-volume histograms can provide insight into treatment efficacy and normal organ toxicity.

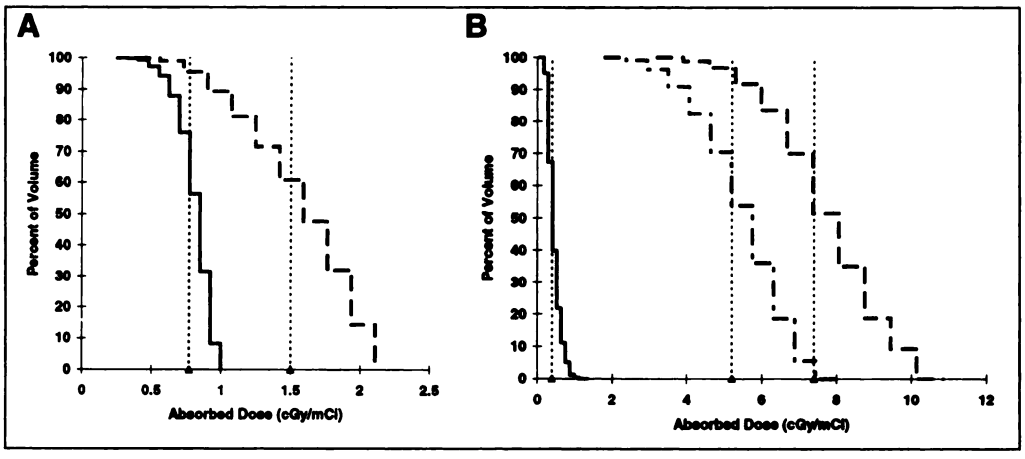

FIGURE 6. Integral dose-volume histograms for Patient 1 [liver self-dose (solid line); spleen self-dose (dashed line)] and Patient 2 [liver (solid line), tumor 1 (dashed and dotted line), tumor 2 (dashed line)], show the percent volume of the tissues receiving a dose equal to or less than the dose (in centigray) on the x-axis. Mean dose for each histograms is shown by a dotted vertical line with a triangle on the x-axis intercept.

ACKNOWLEDGMENTS

We thank Michael G. Stabin of the Oak Ridge Associated Universities for assistance in the S-factor validation studies. This work was supported, in part, by the Frank J. Scallon Medical Science Foundation and by NIH grant nos. RO1 CA62444 and UO1 CA58260, and DOE grant no. DE-FG02-86ER-60407.

REFERENCES

1. Snyder WS, Ford MR, Warner GG, Watson EB. "S," absorbed dose per unit cumulated activity for selected radionuclides and organs. *MIRD Pamphlet No. 11*. New York: Society of Nuclear Medicine; 1975.
2. Snyder WS, Ford MR, Warner GG. Estimates of specific absorbed fractions for photon sources uniformly distributed in various organs of a heterogeneous phantom. *MIRD Pamphlet No. 5, Revised*. New York: Society of Nuclear Medicine; 1978.
3. Loevinger R, Budinger TF, Watson EE. *MIRD Primer for Absorbed Dose Calculations*. New York: Society of Nuclear Medicine; 1991.
4. Leichner PK, Kwok CS. Tumor dosimetry in radioimmunotherapy: methods of calculation for beta particles. *Med Phys* 1993;20:529–534.
5. Meredith RF, Johnson TK, Plott G, et al. Dosimetry of solid tumors. *Med Phys* 1993;20:583–592.
6. Stabin MG. MIRDOSE—the personal computer software for internal dose assessment in nuclear medicine. *J Nucl Med* 1996;37:538–546.
7. Johnson TK. MABDOS: a generalized program for internal radionuclide dosimetry. *Comput Methods Programs Biomed* 1988;27:159–167.
8. Sgouros G, Chiu S, Pentlow KS, et al. Three-dimensional dosimetry for radioimmunotherapy treatment planning. *J Nucl Med* 1993;34:1595–1601.
9. Erdi AK, Wessels BW, DeJager R, et al. Tumor activity confirmation and isodose curve display for patients receiving iodine-131-labeled 16.88 human monoclonal antibody. *Cancer* 1994;73:(suppl):932–944.
10. Sgouros G, Barest G, Thekkumthala J, et al. Treatment planning for internal radionuclide therapy: three-dimensional dosimetry for nonuniformly distributed radionuclides. *J Nucl Med* 1990;31:1884–1891.
11. Giap HB, Macey DJ, Bayouth JE, Boyer AL. Validation of a dose-point kernel convolution technique for internal dosimetry. *Phys Med Biol* 1995;40:365–381.
12. Giap HB, Macey DJ, Podoloff DA. Development of a SPECT-based three-dimensional treatment planning system for radioimmunotherapy. *J Nucl Med* 1995;36:1885–1894.
13. Tagesson M, Ljungberg M, Strand SE. Transformation of activity distribution in quantitative SPECT to absorbed dose distribution in a radionuclide treatment planning system [Abstract]. *J Nucl Med* 1994;123P.
14. Furhang EE, Chui CS, Sgouros G. A Monte Carlo approach to patient-specific dosimetry. *Med Phys* 1996;23:1523–1529.
15. van Dieren EB, van Lingen A, Roos JC, Teule GJJ. Validation of the distance histogram technique for three-dimensional and two-dimensional dosimetric calculations. *Appl Rad Isot* 1992;43:1211–1221.
16. Kolbert KS, Sgouros G, Scott AM, et al. Dose-volume histogram representation of patient dose distribution in three-dimensional internal dosimetry [Abstract]. *J Nucl Med* 1994;35:123P.
17. Kolbert KS, Sgouros G, Graham MC, Larson SM. Display and analysis of multimodality registered images [Abstract]. *J Nucl Med* 1995;36:125P.
18. Rew R, Davis G, Emmerson S. *NetCDF user's guide. An interface for data access*, version 2.3. Boulder, CO: Unidata Program Center, University Corporation for Atmospheric Research; 1993.
19. Furhang EE, Sgouros G, Chui CS. Radionuclide photon dose kernels for internal emitter dosimetry. *Med Phys* 1996;23:759–765.
20. Prestwich WV, Nunes J, Kwok CS. Beta dose point kernels for radionuclides of potential use in radioimmunotherapy. *J Nucl Med* 1989;30:1036–1046.
21. Simpkin DJ, Mackie TR. EGS4 monte carlo determination of the beta dose kernel in water. *Med Phys* 1990;17:179–186.
22. Leichner PK. A unified approach to photon and beta particle dosimetry. *J Nucl Med* 1994;35:1721–1729.
23. Cristy M, Eckerman KF. In: Specific absorbed fractions of energy at various ages from internal photon sources. *ORNL/TM-8381/V1*. Oak Ridge, TN: ORNL 1987.
24. Duda RO, Hart PE. *Pattern recognition and scene analysis*. New York: Wiley; 1973.
25. Caron PC, Jurcic JG, Scott AM, et al. A phase I B trial of humanized monoclonal antibody M195 (anti-CD33) in myeloid leukemia: specific targeting without immunogenicity. *Blood* 1994;83:1760–1768.
26. Pelizzari CA, Chen GTY. Registration of multiple diagnostic imaging scans using surface fitting. In: *Proceedings of the Ninth International Conference on Use of Computers in Radiation Therapy*. 1987:437–440.
27. Sgouros G, Jureidini IM, Scott AM, Graham MC, Larson SM, Scheinberg DA. Bone marrow dosimetry: regional variability of marrow-localizing antibody. *J Nucl Med* 1996;37:695–698.
28. Divgi CR, Scott AM, Dantis L, et al. Phase I radioimmunotherapy trial with iodine-131-CC49 in metastatic colon carcinoma. *J Nucl Med* 1995;36:586–592.
29. Scott AM, Macapinlac H, Zhang JJ, et al. Clinical applications of fusion imaging in oncology. *Nucl Med Biol* 1994;21:775–784.

Patient-Specific Dosimetry Using Quantitative SPECT Imaging and Three-Dimensional Discrete Fourier Transform Convolution

Gamal Akabani, William G. Hawkins, Miriam B. Eckblade and Peter K. Leichner
Department of Radiation Oncology, University of Nebraska Medical Center, Omaha, Nebraska

The objective of this study was to develop a three-dimensional discrete Fourier transform (3D-DFT) convolution method to perform the dosimetry for ^{131}I-labeled antibodies in soft tissues. **Methods:** Mathematical and physical phantoms were used to compare 3D-DFT with Monte Carlo transport (MCT) calculations based on the EGS4 code. The mathematical and physical phantoms consisted of a sphere and a cylinder, respectively, containing uniform and nonuniform activity distributions. Quantitative SPECT reconstruction was carried out using the circular harmonic transform (CHT) algorithm. **Results:** The radial dose profile obtained from MCT calculations and the 3D-DFT convolution method for the mathematical phantom were in close agreement. The root mean square error (RMSE) for the two methods was <0.1%, with a maximum difference <21%. Results obtained for the physical phantom gave a RMSE <0.1% and a maximum difference of <13%; isodose contours were in good agreement. SPECT data for two patients who had undergone ^{131}I radioimmunotherapy (RIT) were used to compare absorbed-dose rates and isodose rate contours with the two methods of calculation. This yielded a RMSE <0.02% and a maximum difference of <13%. **Conclusion:** Our results showed that the 3D-DFT convolution method compared well with MCT calculations. The 3D-DFT approach is computationally much more efficient and, hence, the method of choice. This method is patient-specific and applicable to the dosimetry of soft-tissue tumors and normal organs. It can be implemented on personal computers.

Key Words: Monte Carlo calculations; SPECT; dosimetry; fast Fourier transform

J Nucl Med 1997; 38:308–314

The development of patient-specific dosimetry for administered radionuclides and radiolabeled compounds is essential for a better understanding of tumor response and normal-tissue toxicity. This is particularly relevant in clinical trials in cancer therapy with large administered activities and potentially high radiation-absorbed doses in tumors and normal tissues. As discussed previously, in clinical trials, the absorbed dose is usually calculated rather than measured, and calculations are

Received Nov. 8, 1995; revision accepted Apr. 5, 1996.
For correspondence or reprints contact: Gamal Akabani, PhD, Department of Radiation Oncology, University of Nebraska Medical Center, Box 981045, 600 South 42nd St., Omaha, NE 68198-1045.